SAND2023-10575J

Low threshold, long wavelength interband cascade lasers with high voltage efficiencies

Jeremy A. Massengale, Yixuan Shen, Rui Q. Yang, *Fellow, IEEE*, S. D. Hawkins, and A. J. Muhowski, *Member, IEEE*

***Abstract*—We report on the substantial advancement of long wavelength InAs-based interband cascade lasers (ICLs) utilizing advanced waveguides formed from hybrid cladding layers and targeting the 10-12 µm wavelength region. Modifications in the hole injector have improved carrier transport in these ICLs, resulting in significantly reduced threshold voltages (V_{th}) as low as 3.62 V at 80 K. Consequently, much higher voltage efficiencies were observed, peaking at about 73% at 10.3 µm and allowing for large output powers of more than 100 mW/facet. Furthermore, low threshold current densities (J_{th}) of 8.8 A/cm^2 in cw mode and 7.6 A/cm^2 in pulsed mode near 10 µm were observed; a result of adjustments in the GaInSb hole well composition intended to reduce the overall strain accumulation in the ICL. Furthermore, a second ICL wafer operating at a longer wavelength achieved a peak voltage efficiency of 57% at 11.7 µm, with a peak output power of more than 27 mW/facet. This ICL went on to lase beyond 12 µm in both cw and pulsed modes, representing a new milestone in long wavelength coverage for ICLs with the standard W-QW active region.**

***Index Terms*—Interband cascade lasers, mid-infrared semiconductor lasers, type-II quantum well heterostructures, III-V materials, optical waveguides.**

I. INTRODUCTION

INTERBAND cascade lasers (ICLs) [1] have seen tremendous improvements over the last 20 years, particularly in the 3-6 µm mid-infrared (MIR) window as the leading laser technology for applications [2-7], where low power consumption is key. The type-II ICL utilizes two key design features; 1) photon generation via interband transitions in type-II quantum wells (QWs) that are formed between InAs/GaSb heterostructures and 2) series connected cascade stages that can enhance the total gain (per current density), which were first implemented in the quantum cascade laser (QCL)[8]. In contrast, QCL uses intraband transitions with a very fast phonon scattering, resulting in large threshold current densities required to achieve lasing. However, the interband transitions in ICLs avoid this physical limitation present in the QCL design, and thus ICLs can reach lasing with very low threhold current densities (J_{th}) by comparison. Therefore, the ICL is ideal to target many desirable MIR applications such as free-space communications, chemical sensing, green house gas monitoring, thermal imaging, and industrial process control [9-12].

To date, much of the development for ICLs has been carried out on GaSb substrates, with efficient room temperature (RT) operation demonstrated in the 3-6 µm wavelength (λ) range[5-7]. However, the conventional GaSb-based ICL is poorly suited for longer wavelength operation beyond 6 µm, in part due to the waveguide configuration that is used. In the traditional waveguide for the GaSb-based ICLs, low n-doped GaSb sepearate confinement layers (SCL) surround the cascade active region. Thick InAs/AlSb superlattice (SL) layers are then placed below the bottom SCL and above the top SCL to form the optical cladding. The problem, however, is that at longer wavelengths the optical wave spreads out, and in order to properly confine the light to the gain section, the thickness of the SL cladding must be increased. This presents a challenge for the growth of such devices, which rely on molecular beam epitaxy (MBE). The thicker SL cladding leads to an increased number of shutter movements and also requires more careful control of the relevant beam fluxes during the longer growth time. Also, the InAs/AlSb SL is well known to have a relatively low thermal conductivity (≈ 0.03 W/cmK)[13] that can result in inefficient heat dissapation from the cascade active region, the effect of which is even more impactful at longer wavelengths due to the thicker SL cladding needed.

A clever way to solve this issue is to grow on InAs substrates instead of GaSb substrates, where the low n-doped GaSb SCLs are replaced with undoped InAs SCLs and the InAs/AlSb SLs are replaced with heavily doped n$^+$-InAs plasmon-enhanced cladding layers[14-17]. These plasmon cladding layers provide superior refractive index contrast with the cascade active region, which can enhance the confinement of the optical wave within the gain section. Furthermore, the plasmon cladding has a larger thermal conductivty than the traditional SL, which can help to more efficiently extract heat from the cascade active region at longer wavelengths. This plasmon-enhanced waveguide approach is not limited to the InAs-based ICLs, however. GaSb-based ICLs can also take advantage of this

Manuscript received July xx, 2023. The work at the University of Oklahoma was partially supported by NSF (No. ECCS-1931193). (*Corresponding author: Rui.q.Yang@ou.edu*)

Jeremy A. Massengale was with the School of Electrical and Computer Engineering and the Homer L. Dodge Department of Physics and Astronomy, University of Oklahoma, Norman, OK 73071. He is currently with the U.S. Naval Research Laboratory, Washington, D.C. 20375 (e-mail: jeremy.massengale.ctr@nrl.navy.mil).

Yixuan Shen and Rui Q. Yang are with the School of Electrical and Computer Engineering, University of Oklahoma, Norman, OK 73071 (e-mails: yixuan_shen@ou.edu; rui.q.yang@ou.edu).

S. D. Hawkins and A. J. Muhowski are with Sandia National Laboratories, Albuquerque, NM 87185 (e-mails: sdhawki@sandia.gov; ajmuhow@sandia.gov).

design feature by using heavily n^+-doped InAsSb lattice matched to GaSb, as well as the traditional GaSb SCLs. The main drawback for this design with GaSb-based ICLs is due to the more complicated carrier transport and MBE growth[4,18-20]. The plasmon-enhanced waveguide for InAs-based ICLs has allowed several new milestones to be reached. For example, pulsed lasing above room temperature near 7.1 µm[16] was achieved. Additionally, the InAs-based ICL operation was extended to 11.2 µm, although with a relatively large threshold current density (J_{th}) of 95 A/cm^2 at 80 K and with limited temperature performance[21]. Later, hybrid cladding layers were explored in an advanced waveguide structure and first implemented for InAs-based ICLs operating at a shorter wavelength of 4.6 µm[22]. The advanced waveguide replaces part of the n^+-InAs plasmon cladding with a relatively thin InAs/AlSb SL that is sandwiched between the InAs SCL and n^+-InAs plasmon cladding. This allows for enhanced optical confinement with a simultaneous reduction in the leakage of the optical wave into the high loss plasmon cladding, thus further reducing losses due to free-carrier absorption with a corresponding decrease in the J_{th}. The first implementation of the advanced waveguide into long wavelength InAs-based ICLs operating near 11 µm resulted in a four fold reduction in the J_{th} compared with previous ICLs at similar wavelengths[21, 23]. More recently, redesigned InAs-based ICLs with the advanced waveguide showed an extra two fold reduction in the J_{th} compared with the early work in Ref. 23, and with voltage efficiencies at 80 K of about 53%[24].

In this work we report on the substantial development of long wavelength InAs-based ICLs with advanced waveguides. The results of two 20-stage ICLs with modified cascade active regions based on the results in Ref. 24 are presented, where further reductions in the J_{th} along with enhanced voltage efficiencies and higher maximum operating temperatures are observed. Furthermore, cw emission beyond 12 µm was demonstrated for the first time in these ICLs based on the regular W-QW active region.

II. Design, Growth, and Fabrication of ICL wafers

Two 20-stage InAs-based ICL wafers (EB7902L and EB7910L) were grown with designs similar to that in Ref. 24, but with some adjustments in the cascade region intended to improve the performance for long wavelength operation. Both of the new ICL wafers had slightly thicker GaSb hole injector layers (~ 9.4% and 10.4% in the growth direction) so that the hole levels will shift toward the valence band edge of GaSb and widen the interband tunneling window [25] under a forward bias voltage. As such, the carrier transport through interband tunneling can be improved with a reduced threshold voltage. Both ICLs have a regular W-QW active region which is comprised of a layer sequence of $AlAs_{0.89}Sb_{0.11}$/InAs/GaInSb/InAs/$AlAs_{0.89}Sb_{0.11}$, with thicknesses of 21/35/28/31/12 Å in the growth direction. The GaInSb composition in the hole well is $Ga_{0.65}In_{0.35}Sb$ for ICL wafer EB7910L. For ICL wafer EB7902L, the composition of the GaInSb hole well was changed to $Ga_{0.7}In_{0.3}Sb$ in order to reduce the overall strain accumulation in order to lower the defect density. The increased Ga in the hole well leads to a larger bandgap and a corresponding blue shift in the emission wavelength compared to its counterpart reported here as well as the previous ICLs from Ref. 24. A representative band edge diagram of one cascade period for these ICLs based on a 2-band k·p model[26-27] is shown in Figure 1a.

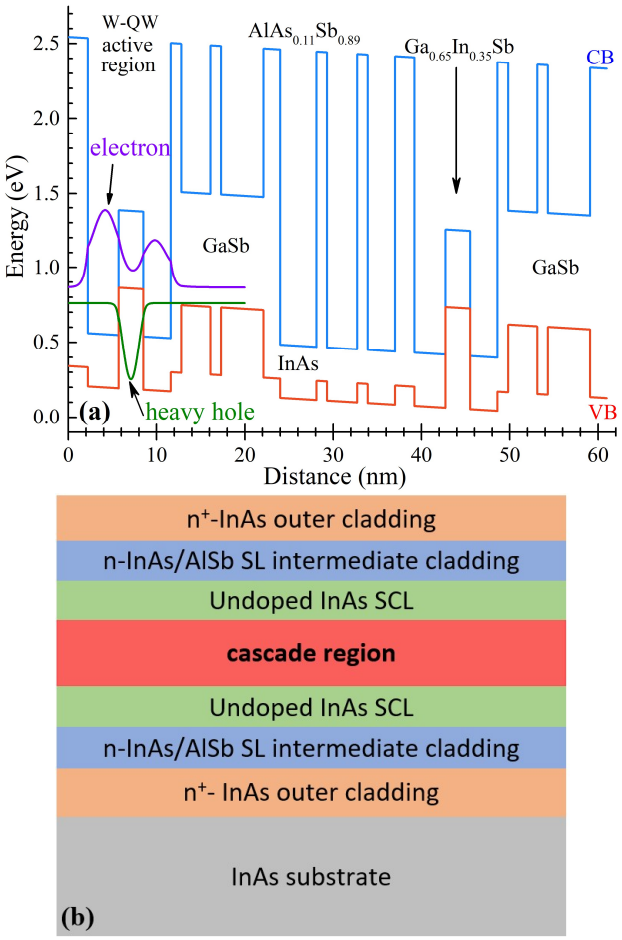

Fig. 1. (a) Band edge diagram for one cascade period of EB7910L, which is representative of the two devices discussed in this work. (b) A schematic diagram of the overall ICL structure showing the various waveguide segments and the cascade active region.

For the waveguide, both ICL wafers had undoped InAs SCLs each with a thickness of 0.98 µm. The ICL wafers included 2.1 µm thick (bottom) and 1.2 µm thick (top) n^+-doped InAs plasmon cladding layers with a doping level of 2.8×10^{18} cm^{-3} and 1.73 µm (bottom and top) n-type InAs/AlSb SL intermediate cladding layers as shown in Figure 1b. As in the previous design from Ref. 24, there are two segments with different doping levels in each of the SL cladding layers in order to further reduce losses due to free-carrier absorption. The segment that is in closer proximity to the cascade region is designed to have a larger refractive index (real part) than the second segment that is closer to the plasmon cladding (as shown in Fig. 8). This is achieved by using a doping level that is a factor of two lower compared to the second segment where InAs layers were doped with Si at 2.3×10^{17} cm^{-3}. This design

choice is to shrink the optical wave penetration into the plasmon cladding, which can further reduce losses due to free-carrier absorption and consequently decrease the required threshold gain to achieve lasing.

The ICL wafers reported in this work were grown by solid-source MBE. The growth temperature used for the strucutres was nominally 440 °C, with growth rates of approximately 0.49 µm/hr for the Sb-containing SL structures (GaSb, GaInSb, AlAsSb) and 1.0 µm/hr for InAs. During the InAs/AlSb SL cladding growth, the As source valve was left open during the AlSb layer growth. Since the As shutter does not fully block the As flux, residual As in the chamber was incorporated into the AlSb layers on the order of about 10%-11%. This feature was accounted for in the design in order to achieve proper lattice matching conditions during the growth calibration. During critical portions of the cascade active region growth, however, the As source valve was closed to avoid any potential incorporation which could affect the lasing characteristics of the devices.

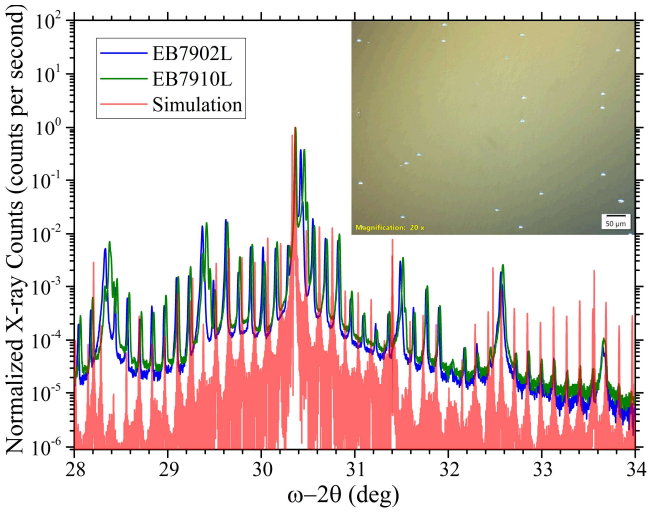

Fig. 2. Measured XRD patterns for EB7902L (Blue) and EB7910L (Green) compared to the simulated pattern (Red). The inset shows the DIC imaging of the surface of EB7902L at 20× magnification where a low density of defects is observed.

X-ray diffraction (XRD) was conducted using a Panalytical X'Pert3 XRD system to asscess the material quality and differential interference contrast (DIC) microscopy was used to characterize the surface morphology of the grown ICL wafers. The XRD scans were taken normal to the (004) axis (symmetric ω-2θ scans) where the resulting XRD patterns of the grown ICL wafers show reasonable agreement with the simulated patterns, as detailed in Figure 2. The strain in the InAs/AlSb SLs of both ICL wafers show as slightly tensile, corresponding to a lattice mismatch of 0.17%-0.28% in the two ICL wafers. Compared to the intended design, the thickness of the InAs/AlSb SL between each of the ICL wafers varied from 0.8% thinner to 1.6% thicker. In both of the ICL wafers, the cascade active region was about 1.5%-1.7% thicker, compared with the design. From DIC surface images (inset in Figure 2) of the two wafers, typical oval hillock defects were observed with each of the ICL wafers having average surface defect densities of 5.7×10^3 cm^{-2} and 1.5×10^4 cm^{-2} for EB7902L and EB7910L, respectively. Besides the standard variation in MBE grown structures, the lower defect density observed for EB7902L could be attributed to the change in the GaInSb hole well composition based on the perspective of reduced overall strain accumulation across the entire structure. The two recently grown ICL wafers exhibited an average defect density that is lower than the previously reported ICLs in Ref. 24 by about a factor of two, indicating good control of the MBE growth parameters.

The grown wafers were fabricated into 100-µm-wide (e.g., EB7902LBA1-1A and EB910LBA1-1A) and 150-µm-wide (e.g., EB7902LBA1-1D and EB7910LBA1-1D) broad area (BA) mesas for quick measurement turnaround using wet chemical etching and standard UV contact photolithography. The wafers were cleaved into approximately 1.5-mm-long (cavity length L_{cavity}) laser bars without substrate thinning and facet coating, which were mounted on copper heat sinks with epi-side up for testing.

III. Device Performance Results and Discussion

Emission spectra of the fabricated ICLs were obtained to using a Nicolet 8700 Fourier transform infrared spectrometer (FTIR). A PM3 Coherent PowerMax thermopile power meter was used to collect the cw output power of ICLs, in which the beam divergence loss was not included. Hence, the reported output power and EQE of the devices presented later are conservative. As shown in Figure. 3, multiple devices from both ICL wafers were able to operate in cw and pulsed modes.

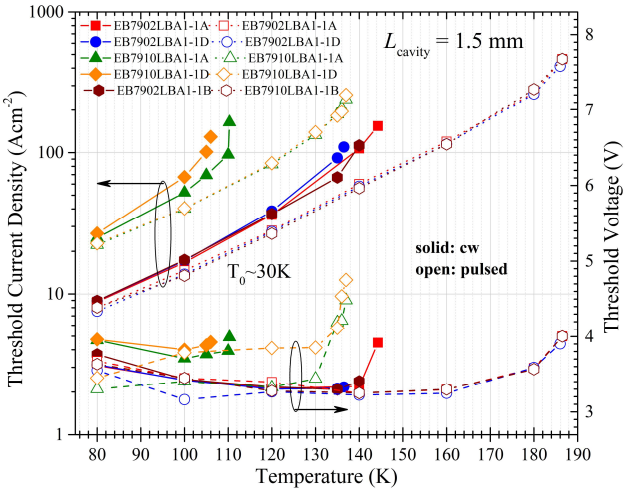

Fig. 3. Threshold current density (J_{th}) and threshold voltage (V_{th}) as a function of temperature for devices from the two wafers.

A. EB7902L Performance Results

In cw mode, three devices (EB7902LBA1-1A, (EB7902LBA1-1B and EB7902LBA1-1D) from the first ICL wafer, which had the modified and less strained GaInSb hole well composition in the W-QW active region, lased with quite similar characteristics as shown in Figure 3. They operated at 80 K with J_{th} values as low as 8.8 A/cm^2, which is reduced by

about 27% compared to the previous ICLs with a slightly longer wavelength (10.2 μm) from Ref. 24. This low threshold current density indicates a good material quality with weak Shockley-Read-Hall (SRH) recombination that is consistent with the lower defect density observed in this wafer. At 80 K, the emission wavelength was about 9.82 μm, 0.4 μm shorter compared to that of previous ICLs with similar designs (10.2 μm at 80 K) [24], which is mainly attributed to the GaInSb hole well composition change mentioned above. These devices also showed a reduced V_{th} as shown in Figure 3 (e.g., 3.62 V at 80 K) compared to the previous ICLs (~4.6 V at 80 K), with their voltage efficiencies peaking at about 73% at 120 K and with a lasing wavelength near 10.3 μm (up from ~ 53% [24]). The voltage efficiency is calculated as $\eta_v = (N_c hc)/(\lambda e V_{th})$ where N_c is the number of cascade stages, h is Planck constant, c is speed of light, e is the electron charge, and λ and V_{th} are the measured emission wavelength and threshold voltage at a given operating temperature. This result is close to that ~ 80% observed in early InAs-based ICLs at shorter wavelengths [4], indicating that the carrier transport has been improved in these new ICLs, attributed to the changes in the GaSb hole injector layers. This high voltage efficiency is of more significance considering that the photon energy is small at such a long wavelength.

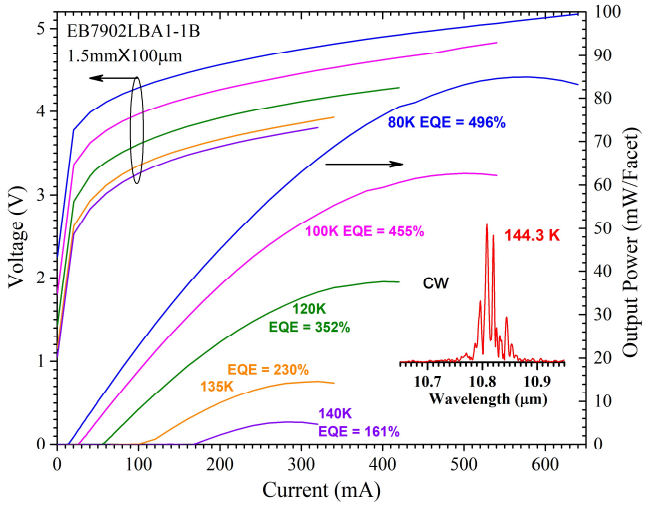

Fig. 4. The CW IVL characteristics for a 100-μm-wide ICL from 80 K to 140 K along with the corresponding EQE values and with an inset showing the cw spectra at its maximum operating temperature.

A representative 100-μm-wide device from the first ICL wafer (EB7902LBA1-1A) went on to operate up to 144.3 K in cw mode, about 20 K higher than the previous ICL in Ref. 21, where it had an emission wavelength of 10.81 μm (inset, Figure 4) and a J_{th} = 154 A/cm^2. Another 100-μm-wide device EB7902LBA1-1B exhibited a maximum cw output power of about 85 mW/facet at 600 mA and 80 K and with an extracted external quantum efficiency (EQE) of 496%, dropping to 161% at 140 K, as shown in the current-voltage-light (IVL) characteristics in Figure 4. The maximum cw output power observed for this device was about 52% larger than the previously reported ICL [24]. Meanwhile, a 150-μm-wide device (EB7902LBA1-1D) operated up in cw mode to 136.5 K and at a slightly shorter wavelength (10.7 μm) and lower J_{th} of 109.4 A/cm^2 due to more heating with the larger size device and more current injection. At 80 K, this 150-μm-wide device delivered an even higher cw output power of 109 mW/facet at 700 mA with a similar EQE to the 100-μm-wide device. Compared to previous ICLs at similar wavelengths, the much higher obtainable output power for these new ICLs was a direct consequence of the reduced heat generation with a high voltage efficiency.

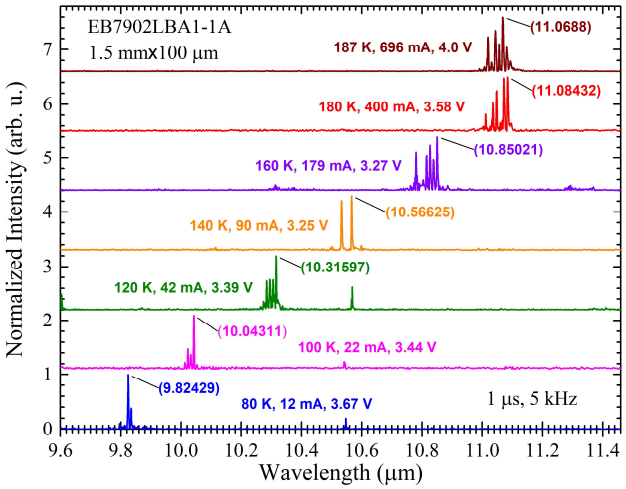

Fig. 5. The pulsed lasing spectra along with the injection current, operating voltage, and lasing wavelength at each temperature step.

In pulsed mode, the 80 K J_{th} was slightly smaller, with measured values of 8 A/cm^2 and 7.6 A/cm^2 for the 100- and 150-μm-wide devices, respectively. Devices A and D were able to operate up to 187 K, and with emission at 11.1 μm along with threshold current densities of 464 A/cm^2 and 412.4 A/cm^2, respectively. A representative temperature dependent emission spectrum for EB7902LBA1-1A is shown in Figure 5. When the heat sink temperature was raised from 180 to 187 K, the lasing wavelength was slightly blue-shifted, indicating the first observation of the band filling effect [28] in these LW InAs-based ICLs with the regular W-QW active region. This blue shift also suggests that the operating temperature T was approaching the maximum limit, during which, the threshold current density J_{th} and voltage V_{th} increased rapidly as shown in Figure 3. In the temperature range of 80 K to 140 K, away from its maximum operating limit, the J_{th} approximately followed an exponential function of T with a characteristic temperature T_0 of ~30 K, which is typical for LW ICLs [24]. The extracted EQE under pulsed operation reached a similar value compared with cw operation, then slowly dropped to 250% at 160 K before decreasing more rapidly to 85% at 180 K, where the voltage efficiency observed in these devices was still relatively high (~ 56-57%). Similar to previously reported InAs-based ICLs [23-24], the maximum allowable J_{th} was significantly lower at the maximum operating temperature compared to their short wavelength counterparts [4,22]. Curiously, this feature is absent in LW InAs-based ICLs which utilize $InAs_{0.5}P_{0.5}$ barriers in the QW active region [23-24,29], which may imply a possible fundamental difference between these two QW configurations that needs to be further explored in the future.

B. EB7910L Performance Results

Devices from the second ICL wafer (EB7910LBA1-1A and EB7910LBA1-1D), which had the more strained $Ga_{0.65}In_{0.35}Sb$ hole well composition in the W-QW active region, lased at 80 K with wavelengths of 11.4 µm and 11.3 µm, J_{th} of 24.9 A/cm^2 and 26.8 A/cm^2, and V_{th} of 3.95 V and 3.96 V, respectively. This result is comparable to the J_{th} of the previously reported ICLs [24] operating at slightly shorter wavelengths (~10.9 µm at 80 K), but with reduced V_{th} (3.95 V vs 4.9 V at 80 K). Considering the similar J_{th} results and the longer operating wavelengths observed in these new ICLs, this further indicates a reduced SRH recombination, consistent with the improved material quality. Its threshold voltage initially decreased with increasing temperature as the bandgap and device electrical resistance decreased with T, and then increased when T approached to the maximum operating temperature as shown in Fig. 3. The voltage efficiency in cw mode peaked at about 57.2% and 55.2% for these devices, which is about 10% larger than the somewhat comparable ICLs from Ref. 24, again validating the improved carrier transport with the modified design even at this longer wavelength. EB7910LBA1-1A and EB7910LBA1-1D reached maximum cw output powers of about 20 mW/facet and 28 mW/facet, respectively, the latter of which is the largest that an interband laser has achieved at such a long wavelength. As shown in Figure 6, EB7910LBA1-1D had an extracted EQE at 80 K of 258%, which then dropped fairly quickly to 78% at 105 K, approaching the maximum cw operation temperature limit of 106 K with a lasing wavelength at 12.02 µm shown in inset of Fig. 6. However, even at this long wavelength of 12 µm, the device was able to deliver a cw output power of 3 mW/facet at 105 K with an injection current of ~300 mA and at an operating voltage of ~4V, which is good enough for sensing in a low temperature environment.

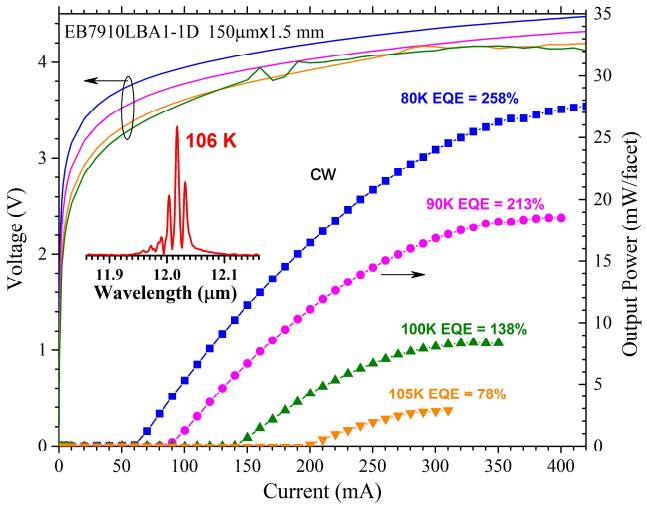

Fig. 6. The CW IVL characteristics for EB7910LBD1-1A from 80 K to 105 K along with the corresponding EQE values and with an inset showing the cw spectra at its maximum operating temperature.

Besides the GaSb hole injector layer thicknesses, devices from this ICL wafer have an identical design to that of a previous ICL in Ref. 21 (EB7541), however their 80 K emission wavelengths are red-shifted by more than 1 µm. This is also longer than the second ICL wafer (EB7547) reported in Ref. 21 with the standard W-QW active region, which had slightly thicker InAs layers of 36.5 Å and 31.5 Å, suggesting that there may be some variations in the QW layer thicknesses between the two growth runs. Nevertheless, the modifications for the GaSb hole injector layer thicknesses and the improved material quality allowed devices from this recent ICL wafer to lase at 80 K with longer emission wavelengths and reduced V_{th}. Both devices (100-µm and 150-µm wide) went on to operate in cw mode up to 110.3 K and 106 K with wavelengths beyond 12 µm, representing a new milestone for ICLs with the regular W-QW active region.

In pulsed mode both devices operated up to 137 K with emission approaching 12.2 µm, which is the longest wavelength achieved for an interband laser with the regular W-QW active region. At their maximum operating temperature, the J_{th} was 240 A/cm^2 and 257.8 A/cm^2 with V_{th} of 4.48 V and 4.75 V, respectively, as shown in Figure 7 for EB7910LBA1-1A. At 137 K, the voltage efficiency had dropped to about 43-45% due to the increased threshold current density and longer wavelength. Similar to the first ICL wafer, devices from the second ICL wafer consistently showed a low maximum allowable threshold current density (the J_{th} at the highest operating temperature at which the device lased), which is more than 5× lower than the $InAs_{0.5}P_{0.5}$ ICLs with similar wavelengths. This behavior appeared to be more significant at longer wavelengths as shown in Fig. 3. Consequently, this severely limited the maximum operating temperature of these ICLs that are based on the regular W-QW active region as well as the longest wavelength that they could reach. What caused such behavior shall be a subject of future research.

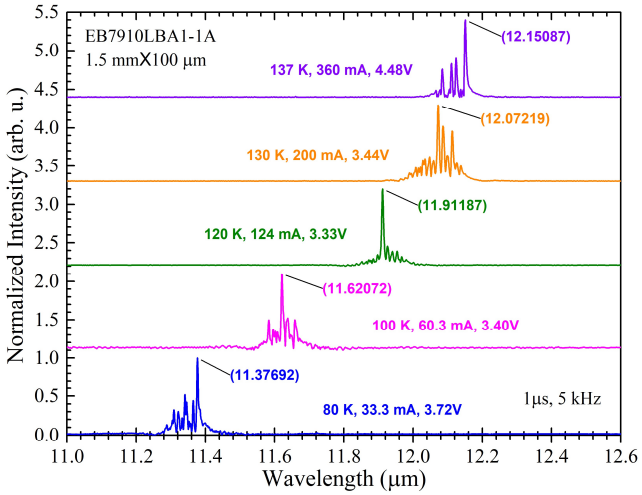

Fig. 7. The pulsed emission spectra for EB7910LBA1-1A along with the operating current, voltage, and emission wavelength at each temperature step.

C. Simulation and Further Discussion

Though the two ICL wafers are structurally similar, differing in design mainly by the composition of the GaInSb hole well in the W-QW active region, the likely variations in the second ICL wafer (EB7910L) led to a longer emission wavelength and

consequently caused a larger free-carrier absorption loss as estimated from the waveguide simulation in Figure 8, which shows the simulated optical wave profile and refractive index for EB7902L (blue) and EB7910L (red). Shown in the figure are the calculated free-carrier loss (α_i), optical confinement factor (Γ), and the effective refractive index of the waveguide (n_{eff}) for the two ICL wafers using their measured 80 K emission wavelengths. Based on the waveguide simulations, the addition of the segmented doping in the SL intermediate cladding results in a decrease in the free-carrier loss from α_i = 4.7 cm^{-1} to 4.0 cm^{-1} and α_i = 7 cm^{-1} to 5.8 cm^{-1} for EB7902L and EB7910L, respectively. The corresponding reductions in the predicted threshold gains (without including other possible losses such as absorption due to intersubband transitions in the valence band) because of this are g_{th} = 51.02 cm^{-1} to 48.41 cm^{-1} and g_{th} = 63.01 cm^{-1} to 58.85 cm^{-1} for 1.5-mm-long devices. This segmented doping in the SL intermediate cladding has a larger impact on devices from EB7910L, because devices from it lase at longer wavelengths compared with devices from EB7902L and hence more of the optical wave penetrates into the plasmon cladding causing it to be more susceptible to free-carrier absorption loss. Furthermore, the free-carrier loss tends to be higher in devices from this ICL wafer because the lasing wavelength is closer to the plasma wavelength (λ_p), which is estimated to be about 14.52 µm from a 3-band model at 80 K. Consequently, the measured J_{th} in both cw and pulsed mode were larger, with the peak voltage efficiency, cw output power, extracted EQE, and overall temperature coverage somewhat lower for devices from this wafer than for those from EB7902L as reflected in Figures 3-7.

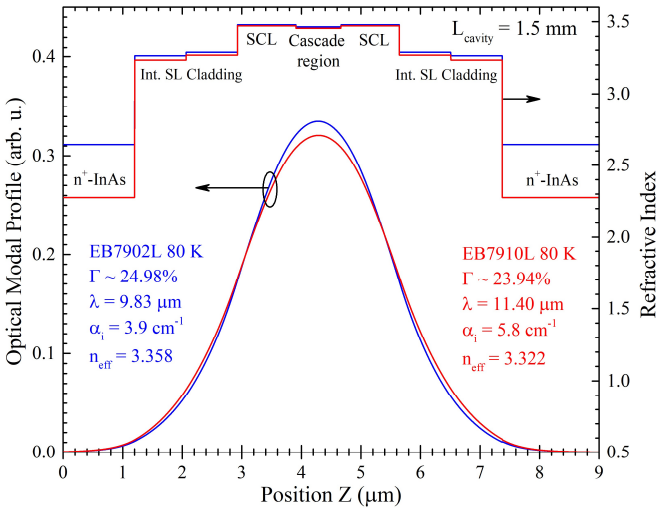

Fig. 8. The calculated optical modal profile and refractive index for (blue) EB7902L and (red) EB7910L, which were generated based on their 80 K emission wavelengths.

V. Conclusion

By modifying the hole injector, LW InAs-based ICLs have been demonstrated with reduced threshold voltages, corresponding to notably increased voltage efficiencies (e.g., 73%) compared to previous ICLs at similar wavelengths. This high voltage efficiency is of particular significance considering the low photon energy (0.12 eV) at this long wavelength (~10.3 µm). Consequently, a high cw output power (>100 mW/facet) was obtained with reduced power consumption. Also, by reducing the local strain with the $Ga_{0.70}In_{0.30}Sb$ hole well to minimize the SRH recombination, a threshold current density below 8 A/cm^2 was achieved at 80 K. Furthermore, the lasing wavelength of ICLs based on regular W-QW active regions has been extended beyond 12 µm in both cw and pulsed modes, far exceeding the traditional boundary for III-V interband lasers. However, on the other hand, the maximum allowable threshold current density is drastically lower with the increase of lasing wavelength compared to shorter wavelength ICLs and those utilizing InAsP barriers in the W-QW active region. This limited the maximum achievable operating temperature and the longest wavelength that the ICLs could reach. This behavior could be related to the reduced gain in type-II W-QWs at long wavelengths and/or increased absorption loss due to intraband transitions in the valence band. As such, the slow increase of the optical gain with more injection of current at higher temperatures or longer wavelengths would be outpaced by a possibly fast increase of the optical loss, making it impossible to lase. The former issue can be alleviated by using the recently proposed QW active region that includes InAsP barrier layers as demonstrated by us [23-24, 29]. The latter may be mitigated by quantum-engineering the valence band QW in the active region as validated recently for ICLs near 5 and 6 µm [6-7]. Hence, by combining both approaches with other possible innovations, ICLs are expected to have substantially improved performance in a wide wavelength region particularly at wavelengths beyond 8 µm where ICLs have not yet achieved operation at room temperature.

Acknowledgment

This work was performed, in part, at the Center for Integrated Nanotechnologies, an Office of Science User Facility operated for the U.S. Department of Energy (DOE) Office of Science. This article has been authored by an employee of National Technology & Engineering Solutions of Sandia, LLC under Contract No. DE-NA0003525 with the U.S. Department of Energy (DOE). The employee owns all right, title and interest in and to the article and is solely responsible for its contents. The United States Government retains and the publisher, by accepting the article for publication, acknowledges that the United States Government retains a non-exclusive, paid-up, irrevocable, world-wide license to publish or reproduce the published form of this article or allow others to do so, for United States Government purposes. The DOE will provide public access to these results of federally sponsored research in accordance with the DOE Public Access Plan https://www.energy.gov/downloads/doe-public-access-plan.
We thank Zhisheng Shi for lending an MCT detector used for the pulsed power testing.

REFERENCES

[1] R. Q. Yang, "Infrared laser based on intersubband transitions in quantum wells," Superlattices Microstruct. 17, 77 (1995).
[2] R. Q. Yang, "Interband cascade (IC) lasers," in Semiconductor Lasers Fundamentals and Applications, edited by A. Baranov and E. Tournie (Woodhead Publishing, Cambridge, 2013), Chap. 12, pp. 487–513.
[3] J. Koeth, R. Weih, J. Scheuermann, M. Fischer, A. Schade, M. Kamp, and S. Höfling, "Mid infrared DFB interband cascade lasers," Proc. SPIE 10403, 1040308 (2017).
[4] R. Q. Yang, L. Li, W. Huang, S. M. Shazzad Rassel, J. A. Gupta, A. Bezinger, X. Wu, G. Razavipour, and G. C. Aers, "InAs-based interband cascade lasers," IEEE J. Sel. Top. Quantum Electron. 25, 1200108 (2019).
[5] J. R. Meyer, W. W. Bewley, C. L. Canedy, C. S. Kim, M. Kim, C. D. Merritt, and I. Vurgaftman, "The interband cascade laser," Photonics 7, 75 (2020).
[6] H. Knotig, J. Nauschutz, N. Opacak, S. Hofling, J. Koeth, R. Weih, and B. Schwarz, "Mitigating valence intersubband absorption in interband cascade lasers", Laser & Photonics Reviews, 2200156 (2022).
[7] J. Nauschutz, H. Knotig, R. Weih, J. Scheuermann, J. Koeth, S. Hofling, and B. Schwarz, "Pushing the room temperature continuous-wave operation limit of GaSb-based interband cascade lasers beyond 6 μm", Laser & Photonics Reviews, 2200587 (2023).
[8] J. Faist, F. Capasso, D. L. Sivco, C. Sirtori, A. L. Hutchinson, and A. Y. Cho, "Quantum cascade laser", *Science* **264**, 553 (1994).
[9] I. Vurgaftman, P. Geiser, W. W. Bewley, C. D. Merritt, C. L. Canedy, M. V. Warren, M. Kim, C. S. Kim, and J. R. Meyer, "Sensitive chemical detection with distributed feedback interband Cascade lasers," in Encyclopedia of Analytical Chemistry, edited by R. A. Meyers (Wiley, Chichester, 2016).
[10] J. Scheuermann, P. Kluczynski, K. Siembab, M. Straszewski, J. Kaczmarek, *et al*, "Interband Cascade Laser Arrays for Simultaneous and Selective Analysis of C1–C5 Hydrocarbons in Petrochemical Industry", Applied Spectroscopy **75** (3), 336-342 (2021).
[11] C. S. Goldenstein, R. M. Spearrin, J. B. Jeffries, and R. K. Hanson, "Infrared laser-absorption sensing for combustion gases," Prog. Energy Combust. Sci. 60, 132–176 (2017).
[12] P. Didier, H. Knötig, O. Spitz, L. Cerutti, A. Lardschneider, E. Awwad, D. Diaz-Thomas, A. N. Baranov, R. Weih, J. Koeth, B. Schwarz, and F. Grillot, "Interband cascade technology for energy-efficient mid-infrared free-space communication," Photon. Res. **11**, 582 (2023).
[13] W. L. L. T. Borca-Tasciuc, D. Achimov, "Thermal conductivity of InAs/AlSb superlattices," Microscale Thermophysical Engineering, vol. 5, pp. 225–231, July 2001.
[14] Z. Tian, R. Q. Yang, T. D. Mishima, M. B. Santos, R. T. Hinkey, M. E. Curtis, and M. B. Johnson, "InAs-based interband cascade lasers near 6 μm," Electron. Lett. 45, 48 (2009).
[15] Z. Tian, R. Q. Yang, T. D. Mishima, M. B. Santos, and M. B. Johnson, "Plasmon-waveguide interband cascade lasers near 7.5 μm," IEEE Photonics Technol. Lett. 21, 1588 (2009).
[16] M. Dallner, F. Hau, S. Hofling, and M. Kamp, "InAs-based interband cascade lasers emitting around 7 μm with threshold current densities below 1 kA/cm^2 at room temperature," Appl. Phys. Lett. 106, 041108 (2015).
[17] R. Q. Yang, L. Li, L. Zhao, Y. Jiang, Z. Tian, H. Ye, R. T. Hinkey, C. Niu, T. D. Mishima, M. B. Santos, J. C. Keay, M. B. Johnson, and K. Mansour, "Recent progress in development of InAs-based interband cascade lasers," Proc. SPIE 8640, 86400Q (2013).
[18] C. L. Canedy, M. V. Warren, C. D. Merritt, W. W. Bewley, C. S. Kim, M. Kim, I. Vurgaftman, and J. R. Meyer, "Interband cascade lasers with longer wavelengths," Proc. SPIE 10111, 101110G (2017).
[19] Y. Lin, J. A. Massengale, W. Huang, R. Q. Yang, T. D. Mishima, and M. B. Santos, "Examination of the durability of interband cascade lasers against structural variations," J. Infrared Millimeter Waves 39, 137 (2020).
[20] J. A. Massengale, Y. Shen, R. Q. Yang, T. D. Mishima, and M. B. Santos, "Interband cascade lasers with advanced waveguides operating in the 3-4 μm wavelength region," Optical Engineering, **62**, 086103 (2023).
[21] L. Li, H. Ye, Y. Jiang, R. Q. Yang, J. C. Keay, T. D. Mishima, M. B. Santos, and M. B. Johnson, "MBE-grown longwavelength interband cascade lasers on InAs substrates," J. Cryst. Growth 425, 369 (2015).
[22] L. Li, Y. Jiang, H. Ye, R. Q. Yang, T. D. Mishima, M. B. Santos, and M. B. Johnson, "Low-threshold InAs-based interband cascade lasers operating at high temperatures," Appl. Phys. Lett. 106, 251102 (2015).
[23] J. A. Massengale, Y. Shen, R. Q. Yang, S. D. Hawkins, and J. F. Klem, "Long wavelength interband cascade lasers," Appl. Phys. Lett. 120, 091105 (2022).
[24] J. A. Massengale, Y. Shen, R. Q. Yang, S. D. Hawkins, and J. F. Klem, "Enhanced Performance of InAs-based Interband Cascade Lasers Emitting between 10-13 μm," Semiconductor Science and Technology 38, 025009 (2023).
[25] R. Q. Yang, "Electronic States and Interband Tunneling Conditions in Type-II Quantum Well Heterostructures", J. Appl. Phys. **127**, 025705 (2020).
[26] S.R. White and L.J. Sham, "Electronic Properties of Flat-Band Semiconductor Heterostructures", Phys. Rev. Lett. **47**, 879 (1981).
[27] R. Q. Yang and J.M. Xu, "Analysis of transmission in polytype interband tunneling heterostructures", J. Appl. Phys. **72**, 4714 (1992).
[28] A. P. Ongstad, R. Kaspi, G. C. Dente, M. L. Tilton, R. Barresi, and J. R. Chavez, "Wavelength tuning limitations in optically pumped type-II antimonide lasers", Appl. Phys. Lett., 92, 141106 (2008).
[29] Y. Shen, J. A. Massengale, R. Q. Yang, S. D. Hawkins, and A.J. Muhowski, "Pushing the Performance Limits of Long Wavelength Interband Cascade Lasers using Innovative Quantum Well Active Regions" Appl. Phys. Lett. **123**, 041108 (2023).

Jeremy A. Massengale was born in Dayton, OH, USA. He received the B.S. degree in physics from Wittenberg University, Springfield, OH, USA in 2013. He received the M.S. degree in engineering physics in 2016 and the Ph.D. degree in physics in 2023 from The University of Oklahoma, Norman, OK, USA

From 2016 to 2023 he worked with Dr. Rui Yang and Dr. Michael Santos on the growth, fabrication, and characterization of interband cascade based mid-IR devices at the University of Oklahoma, Norman, OK, USA. He currently holds a National Research Council post-doctoral fellowship at the US Naval Research Laboratory, Washington D.C., USA. His research interests include the development of growth techniques for III-V based superlattice structures, XRD characterization, nanofabrication methods, and optical characterization techniques for mid-IR devices.

Yixuan Shen received his B.S. degree in electrical engineering and automation from Shanghai Ocean University in 2016 and his M.S. degree in electrical engineering from the University of Oklahoma in 2023. He is currently pursuing his Ph.D. degree in electrical engineering at the University of Oklahoma, where he works on interband cascade laser research. His research focuses on optimizing the waveguide structure of mid-IR interband cascade lasers with III-V materials.

Rui Q. Yang (Fellow, IEEE) received his Ph.D. degree in physics in 1987 and is a professor at University of Oklahoma. Prior to joining University of Oklahoma in 2007, he was a Principal Member of Engineering Staff and a Task Manager at the Jet Propulsion Laboratory, California Institute of Technology, Pasadena, California, where he led the development of advanced interband cascade lasers for applications in Earth sciences and planetary explorations. He is a Fellow of Optica and the recipient of 2018 IEEE Photonics

Society Aron Kressel Award. He has authored/co-authored more than 150 articles in peer-reviewed journals.

Samuel D. Hawkins received a BS in Chemical Engineering from New Mexico Institute of Mining and Technology in 2002. He joined the technical staff at Sandia National Laboratories in 2002. His research interests include the molecular beam epitaxy growth of III-V materials and devices.

Aaron J. Muhowski (Member, IEEE) received a B.S. from the University of Wisconsin, Madison, WI, USA, in 2014, and a Ph.D. from the University of Iowa, Iowa City, IA, USA, in 2019. After a post-doctoral fellowship at the University of Texas at Austin, he joined the technical staff at Sandia National Laboratories in 2022. His research interests include the device design, characterization, and epitaxial growth of high-efficiency III-V emitters and detectors.